J. Fluid Mech. (2009), *vol.* 633, *pp.* 485–507.
doi:10.1017/S0022112009007435 Printed in the United Kingdom

Bubble transitions in strongly collapsed elastic tubes

ALEXANDRA HEAP AND ANNE JUEL†

Manchester Centre for Nonlinear Dynamics and School of Mathematics,
The University of Manchester, Manchester M13 9PL, UK

(Received 29 August 2008 and in revised form 30 March 2009)

The selection of long air bubbles propagating steadily in a strongly collapsed fluid-filled elastic tube is investigated experimentally in a benchtop model of airway reopening. Localized regions of strong collapse are likely in the lung, because collapsing fluid-elastic instabilities promote extensive deformation of the airway cross-section beyond the point of opposite wall contact. We find that radical changes in the reopening mechanics occur at this point. We build on the recent identification by Heap & Juel (*Phys. Fluids,* vol. 20, 2008, article no. 081702) of three different steadily propagating bubbles (asymmetric, double-tipped and pointed) that are selected successively for increasing values of the capillary number (Ca, ratio of viscous to surface tension forces) in tubes initially collapsed beyond the point of opposite wall contact. The asymmetric bubble is also observed in less collapsed tubes for small values of Ca, and we show that it bifurcates super-critically from the usual parabolic-tipped bubble as Ca increases. We also characterize the mechanisms underlying the discontinuous transitions between asymmetric and double-tipped bubbles, and double-tipped and pointed bubbles. In particular, we find that the tube must reopen to a critical height for double-tipped bubbles to be selected. The length of the precursor fingers in the double-tipped bubble decreases with Ca, and the bubble loses stability to pointed bubbles when this length is less than the height of the tube at the point where the fingers merge. By contrast with the asymmetric and double-tipped bubbles, the pointed bubble infiltrates the most collapsed part of the tube to yield the rapid reopening of the airway at low pressure, with the potential to reduce ventilation-induced lung damage.

1. Introduction

The initial opening of airways with a newborn's first breath occurs through the propagation of a long air bubble. The rapid removal of the majority of fluid in the lungs prior to birth suggests that the airways are in a strongly collapsed initial state (Bland 1991). Many pulmonary conditions also promote the collapse and occlusion of parts of the lung with viscous fluid, so that mechanical ventilation is required to restore gas-exchange (Grotberg 2001; Grotberg & Jensen 2004). Although the collapse of airways in diseased lungs has not been documented quantitatively, dynamic models of airway collapse find that airway closure occurs on time scales similar to the breathing cycle through fluid-mechanical 'film collapse' or fluid-elastic 'compliant' collapse, as recently reviewed by Heil, Hazel & Smith (2008). The resulting

† E-mail address for correspondence: anne.juel@manchester.ac.uk

collapse is often extensive, so that the opposite walls of the cross-section of the airway make contact. Moreover, a numerical study of the stability of minimal liquid bridges in elastic tubes by Heil (1999) indicates that for lung parameters, the tube adopts a very strongly deformed configuration with opposite wall contact.

Airway reopening can be modelled by the propagation of a long bubble in a liquid-filled collapsed elastic tube, which is an example of a two-phase displacement flow that interacts with the elastic airway. It is governed by the competition between viscous, surface tension and elastic forces. The capillary number, $Ca = \mu U/\sigma^*$, where U is the bubble speed, and μ and σ^* the dynamic viscosity and surface tension of the lining liquid, respectively, corresponds to the ratio of viscous to surface tension forces. The non-dimensional surface tension, $\sigma = \sigma^*/(RK)$, is the ratio of surface tension to elastic forces, based on the bending stiffness K. For a given tube (i.e. a given value of K), the initial transmural pressure can be varied by changing the level of initial collapse, which is measured by the initial dimensionless cross-sectional area, A/A_0, where A is the cross-sectional area of the collapsed tube, $A_0 = \pi R^2$ and R is the inner radius of the undeformed tube. This quantity is associated with the transmural pressure (pressure inside the tube relative to atmospheric pressure) via a constitutive relation known as the 'tube law' (Kamm 1999; Grotberg & Jensen 2004).

Previous experiments on airway reopening have only reported bubbles with the rounded tip characteristic of the displacement of a more viscous fluid (Taylor 1961). In benchtop experiments performed by Gaver, Samsel & Solway (1990), the parabolic-tipped bubble was observed in strongly collapsed tubes that had negligible bending stiffness, so that the fluid–structure interaction arose from the large tension imposed on the end of the tube. A wavy bubble front was noted at the onset of experiments in a two-dimensional geometry by Perun & Gaver (1995), but the non-uniformities decayed as the bubble front propagated. These bubbles are accurately captured by two-dimensional models, which find that they propagate by peeling apart the tube walls (Gaver *et al.* 1996). Peeling bubbles with rounded tips were also obtained from three-dimensional simulations of moderately collapsed airways, which couple nonlinear shell theory to the Stokes flow equations in the absence of gravity (Hazel & Heil 2003). Their dimensionless pressure on the capillary scale (relative to atmospheric pressure), $P = P^* R/\sigma^*$, where P^* is the dimensional bubble pressure, increases approximately linearly with Ca. However, the study focused exclusively on intermediate values of the non-dimensional cross-sectional area, $0.39 \leqslant A/A_0 \leqslant 0.62$, that correspond to initial transmural pressures approximately equal to $-K$.

In this paper, we investigate airway reopening in the limit of strong initial collapse, which is likely to be present in the lungs. We focus principally on levels of collapse such that the cross-section of an empty model airway features opposite wall contact, i.e. $A/A_0 \leqslant (A/A_0)_{owc}$, where $(A/A_0)_{owc} \simeq 0.18$ is the dimensionless cross-section at which its opposite walls first make point contact. Our benchtop model consists of a uniformly collapsed, fluid-filled silicone tube supported by a horizontal rigid plate (Juel & Heap 2007). In the fluid-filled airway, a thin lubrication film remains between opposing boundaries when $A/A_0 \leqslant (A/A_0)_{owc}$. The injection of a constant flow of air at its inlet leads to the steady propagation of a long bubble that reopens the tube. In our experiments, the ratio of surface tension to elastic forces is $\sigma = (3.4 \pm 0.3) \times 10^{-2}$, where the bending stiffness of the tube is determined by rescaling the pressure required to collapse the tube to opposite wall contact, measured in the laboratory, with its value predicted by thin shell-theory (Flaherty, Keller & Rubinow 1972). The value of σ is small because the tube was selected to be sufficiently stiff, so that it would not deform under its own weight when empty. In the most compliant peripheral airways of the

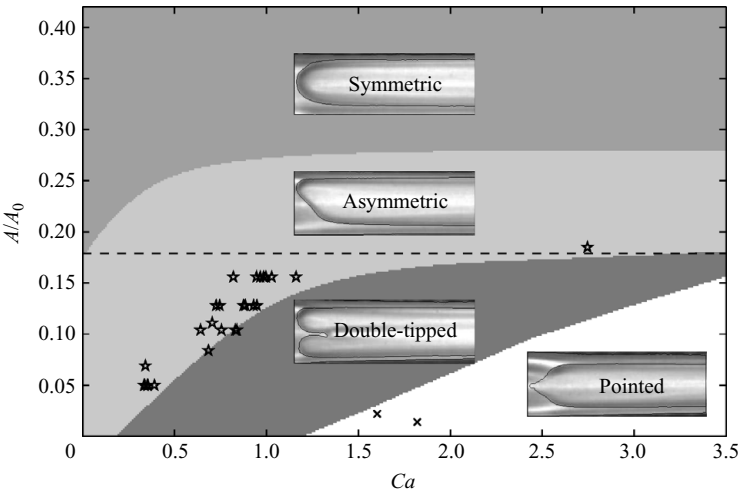

FIGURE 1. Schematic phase diagram in terms of Ca and A/A_0 summarizing the results presented in Heap & Juel (2008). Note that increasing values of A/A_0 correspond to decreasing initial levels of collapse. The value of A/A_0 for which opposite wall contact first occurs, $(A/A_0)_{owc} = 0.18$, is highlighted with a horizontal dashed line. The pentagrams (crosses) correspond to experiments where bubbles formed as double-tipped (pointed) and switched to asymmetric (double-tipped) (see § 3.1.2).

lung, the value of σ is larger by approximately two orders of magnitude. Thus, our experiments do not attempt to mimic lung conditions, but rather aim to demonstrate that the process of reopening a fluid-filled collapsed elastic tube is associated with a considerably wider range of complex dynamics than previously reported. For moderately collapsed tubes, the variation of the non-dimensional surface tension within the range $5 \times 10^{-2} < \sigma < 10$, only shifts the P–Ca curves without altering them qualitatively, as highlighted by the three-dimensional numerical simulations of Hazel & Heil (2003, 2006), and numerical results presented in Juel & Heap (2007) for experimental parameter values. This gives an indication of the robustness of the peeling solution, and suggests that some of our findings in the limit of high collapse may be relevant to higher values of σ.

The combined effects of gravity and of the supporting rigid plate induce an asymmetry in the reopening tube about its horizontal mid-plane. At moderate levels of collapse ($A/A_0 = 0.38$), Juel & Heap (2007) found P–Ca curves that were shifted upwards compared with zero-gravity three-dimensional simulations, and this overall rise in bubble pressure was consistent with two-dimensional results on asymmetric reopening (Jensen *et al.* 2002) and two-dimensional simulations of the effect of gravity (Hazel & Heil 2008). The influence of gravitational forces on the reopening dynamics decreases with increasing level of collapse, as the thickness of the liquid lining in the tube is reduced. The Bond number, $Bo = \rho g \delta^2/(4\sigma^*)$, which measures the ratio of gravity to surface tension forces based on the film thickness δ takes uniformly small values in the range $0.03 \leqslant Bo \leqslant 0.07$ for $0.02 \leqslant A/A_0 \leqslant (A/A_0)_{owc}$ compared with $Bo = 0.5$ for $A/A_0 = 0.41$. Furthermore, the effect of inertial forces is negligible over the range of parameters investigated here (Hazel & Heil 2006; Juel & Heap 2007).

We build on the recent findings of Heap & Juel (2008), who uncovered three novel types of bubbles that propagate steadily in the limit of strong initial tube collapse. Their results are summarized schematically in figure 1. Beyond opposite wall

contact ($A/A_0 \leqslant (A/A_0)_{owc} = 0.18$), the canonical parabolic-tipped bubble is replaced by 'asymmetric', 'double-tipped' and 'pointed' bubbles. These multiple bubble shapes are associated with a discontinuous relationship between bubble pressure and speed, in contrast with the continuous P–Ca relationships that characterize the reopening of less collapsed tubes ($A/A_0 > (A/A_0)_{owc}$). The asymmetric bubbles, whose tip is asymmetric with respect to the vertical mid-plane, and thus displaced from the centre of the tube into one of the side lobes, are also selected for a small range of $A/A_0 > (A/A_0)_{owc}$, and sufficiently large values of Ca.

The pointed bubble is particularly puzzling as it exhibits a cusp-shaped protrusion reminiscent of free-surface entrainment flows (Lorenceau, Restagno & Quéré 2003), and of the free-surface cusps (Courrech du Pont & Eggers 2006) and tips (Cohen & Nagel 2002) that can be formed when withdrawing fluid through a small orifice. Bubbles with a pointed tip also arise in displacement flows of two miscible liquids in rigid tubes (Petitjeans & Maxworthy 1996; Kuang, Petitjeans & Maxworthy 2004) for small bubble speeds. The recirculation flows ahead of the bubble responsible for focusing the interfacial flow also occur in immiscible two-phase displacements at low Ca (Hazel & Heil 2002). However, in Hazel & Heil's simulations (Hazel & Heil 2002), the recirculations did not draw out a pointed tip due to moderating surface tension forces.

Minimal liquid bridges in strongly non-axisymmetrically buckled tubes form double-tipped bubbles, as shown numerically by Heil (1999). His static calculations ($Ca = 0$) were performed by imposing a reflection symmetry about the vertical mid-plane parallel to the tube, so that asymmetric bubbles could not be investigated. The tip symmetry of long bubbles propagating in rigid geometries can be broken by stretching thin wires centrally along the axis of the channel, parallel to the flow direction. By perturbing the free rise of a bubble in a cylindrical tube in this way, Fearn (1988) observed the supercritical breaking of the axisymmetry of the bubble tip as the diameter of the centred wire was increased, with an associated increase in the gravity-driven bubble velocity. In the Hele-Shaw geometry, two symmetrically located wires were required for a sudden jump to an asymmetric state about the vertical mid-plane to occur with increasing Ca. In both configurations, the wire pierced the bubble tip, thus opening a negative angle at the contact point that varied with wire thickness in the first case, and local finger slope via changes in Ca in the second case (Hong 1988). In our airway reopening model, the free surface of the bubble is not perturbed, but the bubble propagation is constrained by the extensive initial deformation of the tube, which is effectively split into two separate channels beyond the point of opposite wall contact.

The aim of this paper is to identify bubble selection criteria in the limit of strong initial tube collapse, and the reopening mechanisms associated with the different bubble shapes. The experimental apparatus is described in § 2.1 with a particular emphasis on bubble visualization and reproducibility, and the collapse of the elastic tube is documented in § 2.2. The variation of P–Ca curves with initial level of tube collapse, discussed in § 3.1, indicates that the point of opposite wall contact sets the threshold between qualitatively different reopening processes. We identify two main reopening regimes in the limit of $A/A_0 \leqslant (A/A_0)_{owc}$ in § 3.2: a peeling mechanism where the bubble pressure is set by viscous stresses in the lobes (asymmetric and double-tipped bubbles), and a fingering mechanism where the work required to open the central region of near-opposite wall contact determines the pressure (pointed bubble). For $A/A_0 \leqslant 0.04$, bubbles with long precursor fingers propagate in the lobes without reopening the tube as discussed in § 3.2.2. The transition between bubbles

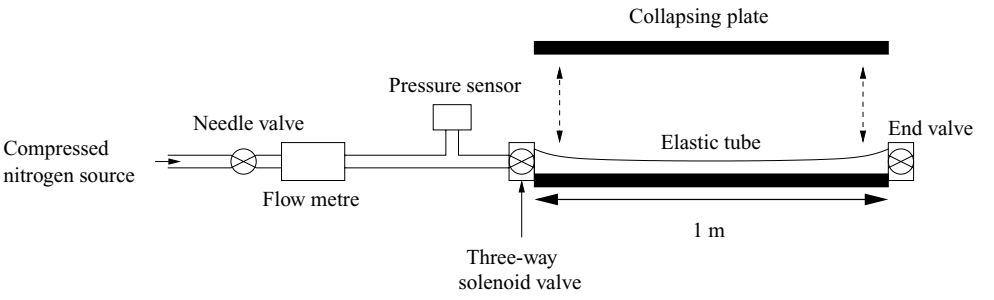

FIGURE 2. Schematic diagram of the experimental apparatus.

are addressed in § 4. For tubes initially collapsed beyond the point of opposite wall contact, all the transitions between bubbles are discontinuous. Simple criteria for the selection of double-tipped bubbles are uncovered from the detailed study of transitions between states. Conclusions are presented in § 5.

2. Experimental methods

2.1. *Description of the apparatus and experimental procedure*

The main features of the experimental apparatus shown schematically in figure 2 are similar to those described in detail in Juel & Heap (2007). Therefore, only essential details are recalled here, but advances in bubble visualization are highlighted in § 2.1.1, and the improved reproducibility following the change of working fluid to paraffin oil is discussed in § 2.1.2.

A 1.0 m long piece of translucent extruded silicone tubing (Primasil Silicones Ltd, Weobley, UK) filled with liquid was positioned on an accurately levelled solid base plate, whose vertical position was held fixed. The base plate was mounted rigidly beneath a facing parallel plate on a vertical translation stage, whose purpose was to collapse the tube mechanically prior to each experiment. The tubing had an inner radius $R = 4.99 \pm 0.16$ mm and a wall thickness $h = 0.57 \pm 0.08$ mm. A manual two-way valve was connected to the downstream end of the tubing. At the upstream end, a three-way pneumatic solenoid valve was used to switch the gas flow from exiting into the atmosphere to entering the tube at the start of each experiment. The flow source was a compressed nitrogen cylinder, whose flow rate was controlled manually by a fine needle valve, and monitored accurately using a mass airflow metre (AWM5000, Honeywell) to range between 50 and 1400 $\mathrm{cm^3\,min^{-1}}$. The flow rate set prior to each experiment could be replicated to within 3 %. At 1400 $\mathrm{cm^3\,min^{-1}}$, the Reynolds number of the air jet flowing out of the solenoid valve nozzle into the tube was approximately equal to 340. Beyond this value the recorded pressure traces showed increasing levels of fluctuations, believed to be due to instabilities in the injected air. Pressure was sampled on personal computer at a rate of 25 Hz from a differential pressure sensor (Honeywell, ± 5 cm H_2O), whose first port was attached to the line immediately upstream of the solenoid valve, while its second port was left open to the atmosphere. The small pressure drop that occurred along the rigid line between the sensor and the inlet of the elastic tube to be reopened was measured directly before mounting the elastic tube. It increased with flow rate and was systematically subtracted in order to yield measurements of the pressure inside the elastic tube.

After carefully filling the tube with liquid following the procedure described in Juel & Heap (2007), the upper plate of the translation stage was lowered onto the

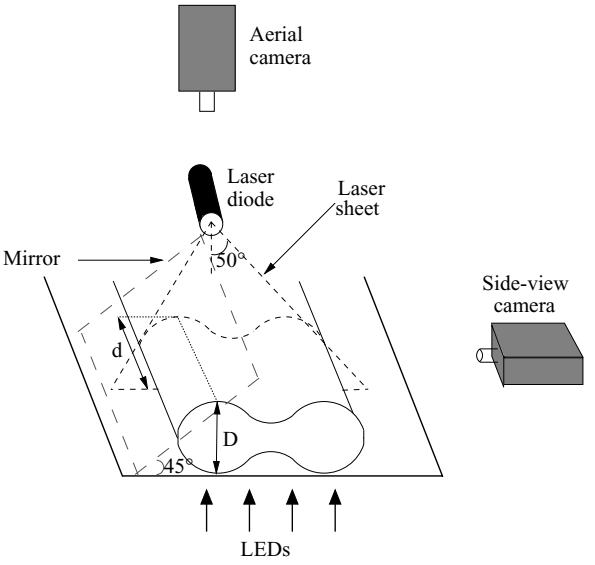

FIGURE 3. Schematic diagram of the visualization set-up. A laser sheet, oriented at 50° from the vertical, is shone onto the deformed tube. The tube is illuminated at different horizontal positions depending on its local height. Thus, the laser sheet outlines local deformations relative to the horizontal base plate, which are captured by the aerial camera. A side-view camera monitors the reopening process and the shape of the advancing bubble via the mirror positioned above the tube at an angle of 45° from the horizontal.

tube in order to collapse it. When the tube was slightly compressed, the downstream valve was opened to evacuate the excess liquid. The position of the upper plate was adjustable to within 0.02 mm, which was less than 2 % of the height of the collapsed tube. Once the desired level of collapse had been reached, the two-way valve was closed to prevent air re-entering the tube. The upper plate was subsequently raised to an adequate height to enable the filming of the reopening process. The tube rapidly relaxed into its equilibrium dumbbell shape, which consisted of two end lobes separated by a thinner central region (see figure 5). After the tube had been filled and collapsed, the solenoid valve was triggered to direct the constant flow of nitrogen into the collapsed fluid-filled tube, and initiate the sampling of both pressure and video footage (see § 2.1.1). This led to the steady propagation of an air bubble, as indicated by the constant bubble pressure recorded during each experiment (see § 2.1.2 and the detailed discussion in Juel & Heap 2007). The steady bubble established rapidly following the decay of short initial transients (within 10 % of the tube length). When the tip of the propagating air bubble reached a position of approximately 5 cm from the end of the tube the pressure rose rapidly, as the injected flow continued to inflate the reopened tube and saturated the pressure sensor. At this point the experiment was discontinued by opening the downstream valve to avoid permanent deformation of the silicone tube.

2.1.1. *Imaging*

A schematic diagram of the imaging system that enabled the capture of three complementary views of the reopening tube is shown in figure 3. The deformation of the top half of the tube was outlined with a laser sheet shining at an angle of 50° from the vertical. The local height of the tube was given by $D = d/\tan 50$, where d

is the displacement of the laser line from its position on the flat base plate, as shown schematically in figure 3. The laser sheet was generated by a laser diode (1.5 mW) fitted with a cylindrical lens. The aerial-view camera captured both the deformed laser line within a 2.5×2.0 cm visualization window at a distance of 25 cm downstream of the inlet, and the outline of the bubble tip as it passed.

A second camera, located 65 cm downstream of the inlet, captured an 8.5 cm long side view of the reopening tube. Movies of the advancing reopening front were analysed to yield a measurement of the average velocity of the propagating air bubble. For each snapshot, the upper boundary of the tube was located by edge detection, and the point where the height of the tube departed from its initial collapsed state was determined to within two pixels, resulting in a relative error on the bubble velocity of less than 2 %. Moreover, constant pressure measurements of steadily propagating bubbles were averaged over the length of this downstream visualization window. The side-view camera also captured top-view images of the advancing bubble, which were reflected by a float glass mirror positioned directly above the tube at an angle of 45°. The visualization section was illuminated from below with a strip of white LEDs, whose brightness could be adjusted. They were chosen for their small heat generation, so that they did not affect the temperature of the fluid on experimental time scales.

These two visualization positions were selected empirically to ensure that transients had decayed at the upstream location, and that the bubble was not affected by the end of the tube at the downstream location, over the entire parameter range investigated. For most of the measurements reported in this paper, the aerial view of the bubble tip did not evolve between these two measurement points and thus, the bubble shape was steady.

The images from the side- and aerial-view cameras were combined using an image inserter (Kramer, PIP-200), and sampled simultaneously onto a personal computer at a rate of 25 frames s^{-1}. A typical snapshot of a reopening experiment is shown in figure 4. The image in the bottom left-hand corner is from the aerial-view camera, and depicts a reopened tube captured after the passage of the bubble. The long side-view and top-view images of the tube, displayed in the remainder of the image, show a bubble that propagates from right to left. The side-view picture reveals the profile of the tube in the transition region between collapsed and reopened states, but the bubble itself is almost undetectable. However, the outline of the bubble is visible in the mirror-reflected top view. Edge detection was performed reliably on many of these top-view bubble images, despite the limited image contrast and sharpness due to unavoidable light scattering by the translucent (semi-opaque) tube. Indeed, although lighting from below resulted in the strongest contrast, it also led to undesirable reflections from the mirror and the tube, which could mask the bubble locally.

2.1.2. *Choice of fluid*

Paraffin oil (Bells, Sons & Co, Widnes, UK) was chosen as the working fluid instead of silicone oil used by Juel & Heap (2007). Silicone oil, which has the advantage of commercial availability in a wide range of viscosities, was found to permeate into the wall of the tubing on short time scales of approximately 3 h. Thus, only six consecutive experiments could be performed on the same section of tube, in order to ensure minimal changes to its elastic properties and the reproducibility of the results. With paraffin oil, the elastic properties of the tube were altered less rapidly, thus enabling the less frequent replacement of the silicone tube (every 3 days), with up to 240 experiments performed on the same section of tube. By avoiding the replacement of the tube during carefully planned parameter studies, the maximum standard deviations

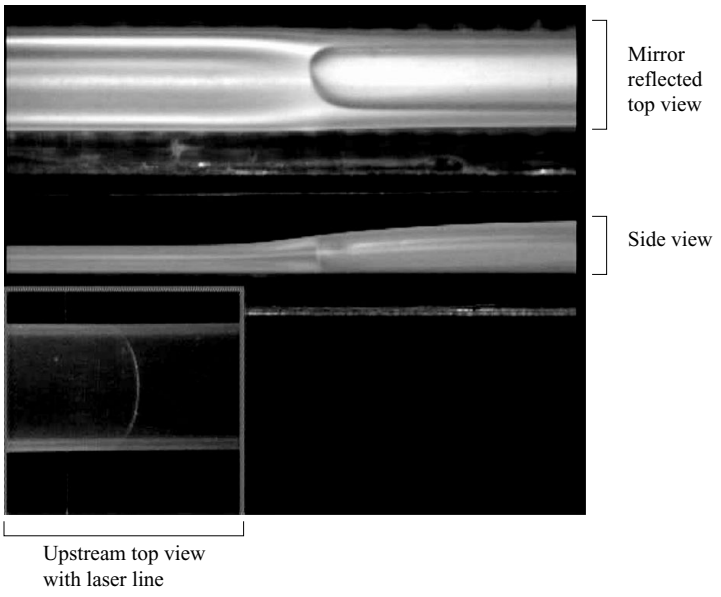

FIGURE 4. Typical snapshot of the reopening process. In the bottom left-hand corner is the aerial-view image with the laser light sheet illuminating the top half of the tube (located 25 cm downstream of the inlet). The bubble tip, travelling right to left, has already passed so the tube is open, as indicated by the concave laser line. The two other images are captured by the side-view camera located 65 cm downstream of the inlet. Immediately above the aerial image is the side view of the tube with the air bubble propagating from right to left. Above this is the mirror image of the upper surface of the tube showing the same tube section as the side view. This image gives a top view of the propagating bubble.

of bubble pressure and Ca (calculated from five repetitions of the experiment) were reduced by factors of four and two, respectively, to $\Delta P = 3$ and $\Delta Ca = 0.05$. These values were calculated over the length of the downstream visualization window described in § 2.1.1. The main source of experimental uncertainty was attributed to the manipulations involved in the replacement of the tube, rather than long-range spatial variations in the properties of the tube. Also, although paraffin oil did not wet the tube perfectly (a contact angle of $55 \pm 3^\circ$ was measured in the laboratory), film de-wetting effects were not observed during the propagation of the bubble. Moreover, the different types of bubbles presented in this paper were also found in experiments with silicone oil, which fully wets the tube. The dynamic viscosity μ, density ρ and surface tension σ^* were measured at the laboratory temperature of $18 \pm 1^\circ$C to be: $\mu = 2.04 \times 10^{-1}\,\mathrm{kg\,m^{-1}\,s^{-1}}$, $\rho = 8.64 \times 10^{3}\,\mathrm{kg\,m^{-3}}$ and $\sigma^* = 2.9 \times 10^{-2}\,\mathrm{N\,m^{-1}}$.

2.2. *Collapse of the elastic tube*

The relationship between the transmural pressure and the cross-sectional area of the tube is shown in figure 5. This 'tube law' was obtained by injecting air at a flow rate of $50\,\mathrm{cm^3\,min^{-1}}$ into a fully collapsed empty tube. The tube reopened slowly and uniformly along its entire length, so that its dimensionless cross-sectional area, A/A_0, was proportional to the time elapsed, as described by Juel & Heap (2007). The range of A/A_0 investigated in this paper is delimited with vertical dashed lines. Examples of cross-sections that combine experimental pictures of the upper half of the tube outlined with a laser line and a schematic representation of the entire cross-section (neglecting gravity) are shown as insets in figure 5. As the tube is compressed, the value

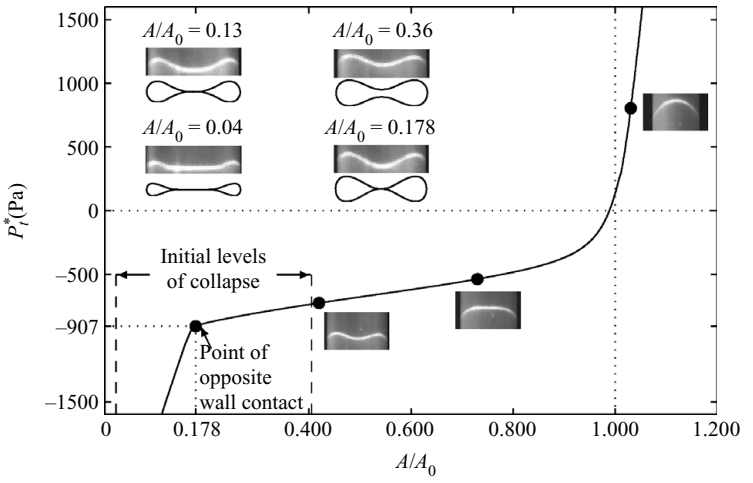

FIGURE 5. Experimentally measured 'tube law': variation of the transmural pressure P_t^* with the cross-sectional area of an empty tube. The pressure at the point of opposite wall contact is $P_{owc}^* = -907$ Pa, which yields a bending stiffness of $K = 173 \pm 4\,\mathrm{N\,m^{-2}}$ following the method detailed in Juel & Heap (2007). The range of initial levels of tube collapse studied ($0.02 \leqslant A/A_0 \leqslant 0.41$) is delimited by vertical dashed lines. Note that the pressure sensor could not capture the large negative transmural pressures of the highest levels of collapse, i.e. $A/A_0 < 0.06$; its pressure range was chosen to maximize the resolution of the bubble pressures.

of the transmural pressure becomes increasingly large and negative. After the tube has buckled and adopted an elliptical cross-section, further small reductions of the inner pressure yield large reductions in A/A_0 until the opposite walls of the cross-section first make contact at $A/A_0 = (A/A_0)_{owc}$. For $A/A_0 < (A/A_0)_{owc}$, which is the range of initial tube collapses of interest in this paper, the tube is almost totally collapsed, and large reductions in inner pressure yield only small reductions in A/A_0. The bending stiffness K was determined by rescaling the pressure of opposite wall contact with the thin-shell theory predictions of Flaherty *et al.* (1972) to be $K = 173 \pm 4\,\mathrm{N\,m^{-2}}$, so that the ratio of surface tension to elastic forces was $\sigma = \sigma^*/(KR) = (3.4 \pm 0.3) \times 10^{-2}$.

2.2.1. *Measurement of* A/A_0

For the reopening experiments, the fluid-filled tube was collapsed by compressing it between parallel plates as described in § 2.1. The cross-section adopted a strained configuration that was approximated by a rectangle with spherical caps, as illustrated in Juel & Heap (2007). As the cross-section retained a constant perimeter, its inner surface area could be calculated based on the separation between the compressing plates, H, to be given by

$$A/A_0 = \left(R - \frac{H}{4} + \frac{h}{2}\right)(H - 2h)R^{-2},$$

where R is the inner radius of the undeformed tube, h the wall thickness. This relation gives values for a compressed tube in the range $0 \leqslant A/A_0 < 1$. Differences between A/A_0 measurements in empty and fluid-filled tubes were minimal (of the order of experimental resolution). The method of strained cross-sections was validated in an empty tube by comparison with the tube law measurements shown in figure 5. The value of the cross-sectional area at the point of opposite wall contact could be read directly from the tube law to be $(A/A_0)_{owc} = 0.178$. To determine $(A/A_0)_{owc}$ with the method of strained cross-sections, lobes heights were measured from images of

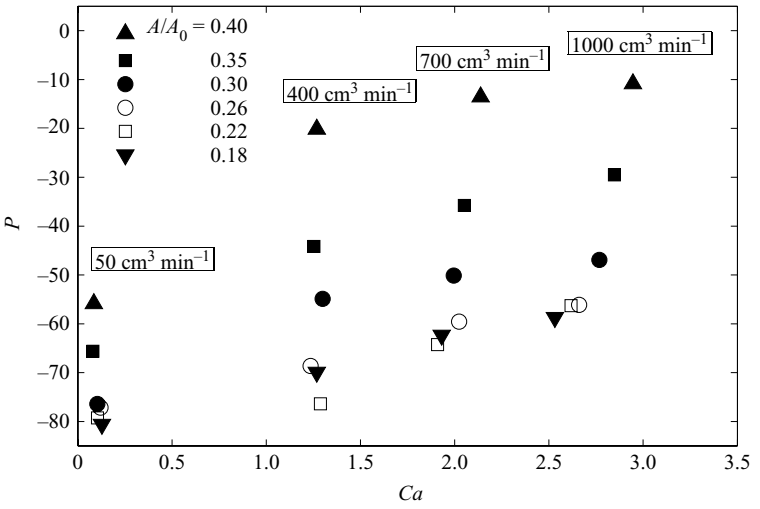

FIGURE 6. Variation of the bubble pressure with Ca for increasing initial level of collapse (i.e. decreasing A/A_0) prior to first opposite wall contact ($(A/A_0)_{owc} = 0.18$).

the deformed tube that was collapsed mechanically to different levels beyond the point of opposite wall contact. The value of the cross-sectional area at the point of opposite wall contact was obtained by linear extrapolation of this data to the lobe height measured at the point of opposite wall contact in the tube law to yield $(A/A_0)_{owc} = 0.173$, confirming the accuracy of the method within 3 %.

3. Bubble pressure variation with A/A_0

3.1. *Critical threshold*

3.1.1. $A/A_0 > (A/A_0)_{owc}$

The variation of bubble pressure with Ca is shown in figure 6 for six values of A/A_0. These initial areas of the collapsed tube are in the range $0.18 \leqslant A/A_0 \leqslant 0.41$ and the steadily propagating bubble is either symmetric or asymmetric as discussed (Heap & Juel 2008). Each point corresponds to a single experimental run, and all the experiments were performed on the same section of tubing at four values of the flow rate of $Q = 50, 400, 700, 1000\,\mathrm{cm^3\,min^{-1}}$. For each value of A/A_0, the pressure increases monotonically with Ca. The P–Ca curves are shifted downwards with decreasing A/A_0, indicating that more collapsed tubes enable the propagation of lower pressure bubbles, which in turn reopen the tube partially to smaller heights. These findings are consistent with the numerical predictions of Hazel & Heil (2003), who found that it was easier to reopen a more collapsed tube because less work was required to redistribute fluid in the tube, the smaller the cross-sectional area ahead of the finger. As $A/A_0 \rightarrow (A/A_0)_{owc}$, the pressure curves tend towards a saturation curve, which is reached for $A/A_0 = 0.26$ to within experimental uncertainty. (This is the largest value of A/A_0 at which we observed asymmetric bubbles). This saturation curve was characterized in further detail by gathering a more extensive set of data for $A/A_0 = 0.26$, which is shown in figure 7(a). Five experiments were performed at each value of Q, and each individual result is included in the figure. Thus, we have not included error bars on these measurements, but the modest scatter gives a measure of the excellent reproducibility of the experiments with paraffin oil, with

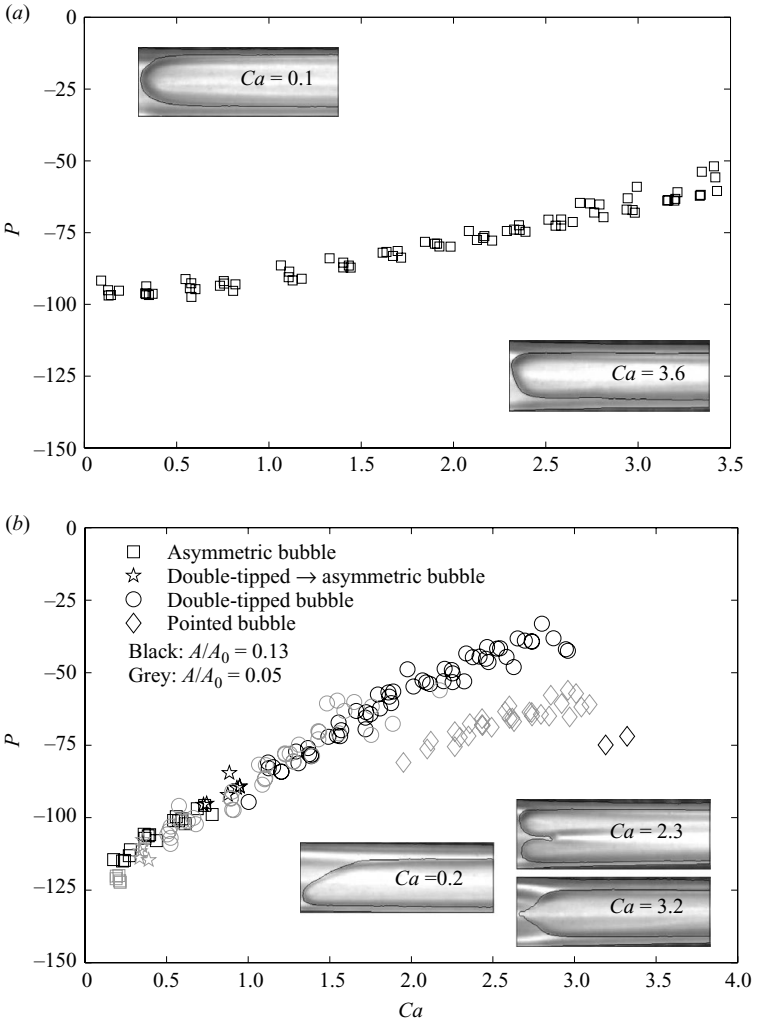

FIGURE 7. Variation of the bubble pressure with Ca: (*a*) $A/A_0 = 0.26$. The insets are top-view images of the bubble at $Ca = 0.1$ (symmetric bubble) and $Ca = 3.6$ (asymmetric bubble). (*b*) $A/A_0 = 0.13$ and $A/A_0 = 0.05$. The insets are top-view images of outlined bubble shapes at $Ca = 0.2$ (asymmetric bubble), $Ca = 2.3$ (double-tipped bubble) and $Ca = 3.2$ (pointed bubble). The reopening states are distinguished with different symbols.

average errors less than $\Delta P = 3$ quoted in § 2.1.2. Note that the section of tube used for these experiments was different from that of figure 6, and that as a result, the minimum dimensionless pressure recorded at $Q = 50\,\mathrm{cm^3\,min^{-1}}$ was reduced by approximately 15 units. In figure 7(*a*), the pressure remains constant at $P = -94 \pm 2$ for $Ca \leqslant 0.8$, and grows monotonically beyond this point. In the region of constant pressure, top-view snapshots indicate the narrowing of the bubbles with increasing Ca, so that a thicker liquid film is left behind on the tube walls after the passage of the bubble tip, similarly to two-phase displacement flows in rigid capillary tubes (Taylor 1961; Bretherton 1961). However, the width of the bubble reaches an approximately constant threshold for $Ca > 0.8$, which coincides with the onset of pressure increase with Ca.

The bubble pressure and capillary number are both influenced by the continuous change in bubble shape from symmetric to strongly asymmetric (see § 4.1). Small reductions in Ca are apparent in figure 6 in the data measured at $Q = 700$ and $1000\,\mathrm{cm}^3\,\mathrm{min}^{-1}$ when A/A_0 decreases. These reflect the propagation of increasingly asymmetric bubbles. While for symmetric bubbles, the dependence of Ca on Q is simply linear, the rate of increase of Ca with Q slows as the tips of the asymmetric bubbles increasingly deform. This is accompanied by an associated growth in bubble pressure, which is consistent with the constant value of Q imposed in each experiment, and translates to a small change in the overall form of the P–Ca curves in figure 6 as $A/A_0 \to (A/A_0)_{owc}$.

3.1.2. $A/A_0 \leqslant (A/A_0)_{owc}$

In figure 7(b), P–Ca data are presented for $A/A_0 = 0.13$ (black symbols) and $A/A_0 = 0.05$ (grey symbols), which were measured on the same section of tube as the data in figure 7(a). As in figure 7(a), five experiments were performed at each value of Q. We chose not to average the results as in Juel & Heap (2007), so that qualitative differences could be identified between the different types of bubbles that were occasionally found for the same value of Q. For these levels of initial collapse, asymmetric, double-tipped and pointed bubbles were observed to propagate steadily as Ca increased. An example of each type of bubble is inset into the figure. The pressures of all three types of bubbles increase approximately linearly with Ca. Double-tipped bubbles succeed asymmetric bubbles as Ca is increased, but both types of bubbles exhibit the same pressure dependence on Ca, so that the transition between these states cannot be detected from the pressure measurements alone. The pressure of the pointed bubble, however, is systematically lower, but grows with Ca at the same rate as that of the two other bubble types. Thus, it lies on a disconnected curve, which is approximately parallel to the pressure curve that includes the asymmetric and double-tipped data. Moreover, the maximum values of Ca for which asymmetric and double-tipped bubbles were observed, both decrease when A/A_0 is reduced as seen in figure 7(b), and these transitions are discussed in § 4.

Occasionally, a double-tipped bubble would form initially, and then switch to an asymmetric bubble during the course of a reopening experiment where the parameters were held fixed. These observations are recorded with pentagrams in figures 7(b) and 1. They form a region of bi-stability between the parameter regions where asymmetric and double-tipped bubbles are selected. The switch was accompanied by a small drop in pressure and tube inflation, and an associated rise in Ca (because each experiment was conducted at constant flow rate). These took place typically over less than 20 % of the experimental run time. Observations were also made of the occasional switch from pointed to double-tipped bubbles within an experiment, marked with black crosses in figure 1. This switch was accompanied by a rise in pressure and drop in Ca, and the variation of these parameters was approximately five times larger than that for the switch from double-tipped to asymmetric bubble (see § 3). These relatively sudden but important changes in bubble properties suggest an exchange of stability between different states (see § 4).

The results presented in this section establish $(A/A_0)_{owc}$ as the threshold between qualitatively different reopening regimes. The novel reopening behaviour for $A/A_0 < (A/A_0)_{owc}$ is closely linked with the important changes in initial tube configuration that occur at $(A/A_0)_{owc}$, where the opposite wall contact splits the collapsed tube into two separate channels.

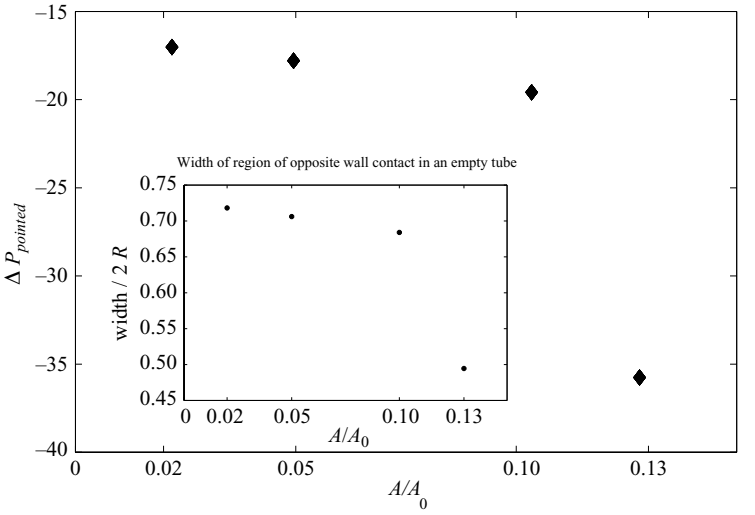

FIGURE 8. Variation of $\Delta P_{pointed}$ with the level of collapse, A/A_0, where $\Delta P_{pointed}$ is the difference between the pressures of the slowest propagating pointed bubble and the fastest double-tipped bubble. The inset shows the width of the region of opposite wall contact in an empty tube as a function of A/A_0.

3.2. *Distinct reopening regimes*

3.2.1. *Pointed bubble versus asymmetric and double-tipped bubbles*

The P–Ca saturation curve shown in figure 7(a) exhibits significant differences from the data taken for $A/A_0 < (A/A_0)_{owc}$ on the same tube. The minimum bubble pressure, measured for the lowest applied value of flow rate, $Q = 50\,\mathrm{cm^3\,min^{-1}}$, is approximately 25 % lower in figure 7(b) than for $A/A_0 = 0.26$ in figure 7(a), and the bubble pressure increases more rapidly with Ca. This reflects qualitative changes in the work required to reopen the tube when A/A_0 is reduced below the first point of opposite wall contact. Whereas for $A/A_0 > (A/A_0)_{owc}$, it becomes easier to reopen the tube as A/A_0 decreases as discussed in § 3.1.1, for $A/A_0 < (A/A_0)_{owc}$, an increase of the work required to reopen the tube is likely for small reductions in A/A_0 because of the increasing shear rates encountered in the thinning liquid films ahead of the bubble. However, the pressures of asymmetric and double-tipped bubbles for $A/A_0 = 0.13$ and $A/A_0 = 0.05$ collapse onto a single curve, and thus appear to be quasi-independent of the level of collapse over this range of A/A_0. This is because these two types of bubbles initiate the reopening process in the lobes of the tube, so that the pressure is determined by the shear rates in these regions. As the lobes do not alter significantly between $A/A_0 = 0.13$ and $A/A_0 = 0.05$, the shear rates are not significantly modified, so the pressure appears independent of A/A_0.

By contrast, the pressure of the pointed bubble depends strongly on the level of collapse. This is because this bubble infiltrates the central region of the cross-section where opposite walls are only separated by thin lubrication films. The central region grows considerably in the transverse direction as A/A_0 is reduced as indicated by the inset of figure 8. The difference in pressure between the slowest propagating pointed bubble and the fastest double-tipped bubble, $\Delta P_{pointed}$, shown in figure 8, exhibits a similar variation with A/A_0. $\Delta P_{pointed}$ is essentially a relative measure of the pressure of the pointed bubble as the pressure of the double-tipped bubble does not vary significantly with A/A_0. Its correlation with the width of the thin-film region suggests

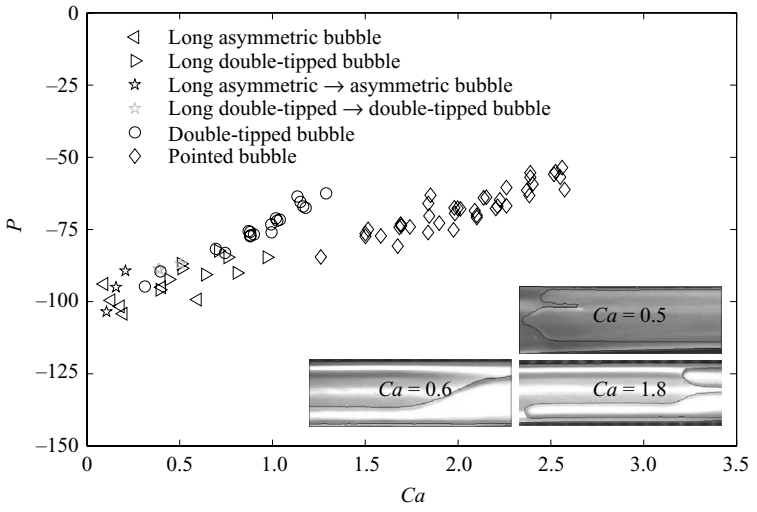

FIGURE 9. Variation of the bubble pressure with Ca for $A/A_0 = 0.02$. The reopening states are distinguished by the use of different symbols. (Insets) Long asymmetric bubble ($Ca = 0.6$), long double-tipped bubble ($Ca = 0.5$) and the mixed double-tipped/pointed bubble ($Ca = 1.8$).

that the pressure of the pointed bubble is set by the work required to peel apart the opposite walls in this central region, which is also proportional to the width of the thin-film region. Note that the collapsed region was easily measured in an empty tube, whereas in the liquid-filled collapsed tube, it was difficult to delimit accurately for technical reasons. However, the shapes of empty and liquid-filled collapsed cross-sections differ only slightly because of the effect of gravity.

3.2.2. *The limit of very strong collapse*

Other novel types of bubbles were encountered in addition to the states reported by Heap & Juel (2008) in the limit of very strong collapse, for $A/A_0 \leqslant 0.04$ and $Ca \leqslant 1.0$. A long narrow bubble propagated steadily through one side lobe, leaving the remainder of the cross-section virtually unaffected by its passage. The tail end of this long finger broadened to form either a long asymmetric or long double-tipped bubble, as illustrated in figure 9 for $A/A_0 = 0.02$, which was the strongest level of collapse that could be reached experimentally. For $A/A_0 = 0.04$ only long asymmetric bubbles were observed in addition to the main bubble states, and they occurred over a range of Ca where double-tipped bubbles were observed for larger values of A/A_0. The very strong initial collapse implies that the upper and lower boundaries of the tube are in contact except within narrow side lobes (see figure 5). The large (negative) initial transmural pressure is sufficient to ensure the isolation of these lobes, so that the propagation of a narrow finger is promoted in either lobe, while the opposite walls of the central part of the cross-section remain in contact. The reopening of the tube only occurs when the precursor finger broadens into the main bubble, in contrast with the double-tipped bubble where opposite wall contact is lost at the tip of the bubble, and a liquid bridge is formed in the central part of the cross-section, which separates the two fingers (Heap & Juel 2008). The length of the precursor finger varied significantly between experiments, in the range 10 %–90 % of the channel length for long asymmetric bubbles, and 5 %–40 % of the channel length for long double-tipped bubbles, suggesting that the precursor finger is very sensitive

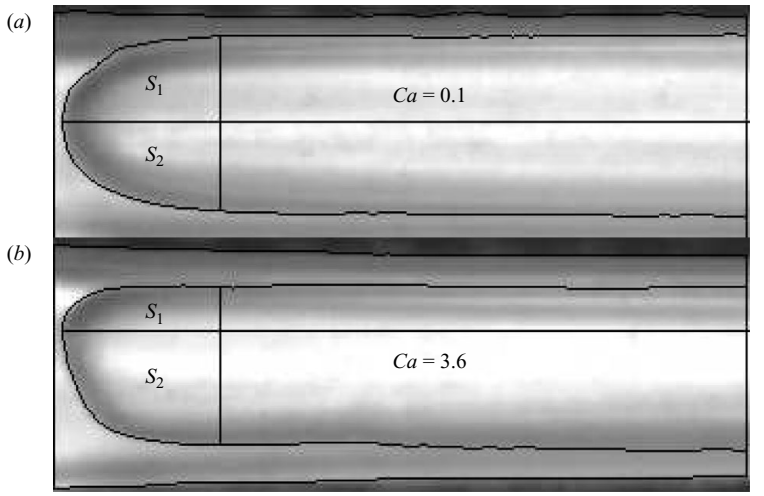

FIGURE 10. Snapshots of steadily propagating bubbles at $A/A_0 = 0.26$. Bubbles are asymmetric about the vertical mid-plane for $Ca > 0.1$, and the tip asymmetry is measured by $\beta = S_2/(S_1 + S_2) - 0.5$, where S_1 and S_2 are the fractional surface areas of the tip shown in the pictures.

to background fluctuations. The average finger length is reduced with increasing Ca as increasing viscous forces are able to counteract the strong elastic forces, and reopen the tube over shorter distances.

The pressure data measured for $A/A_0 = 0.02$ can be seen in figure 9 to be qualitatively similar to that shown in figure 7(*b*) for $A/A_0 = 0.13$ and $A/A_0 = 0.05$. At least five experiments were performed for each value of Q, and all the results are shown on the graph. Note that even in this limit of almost complete collapse, a pressure step remains between the double-tipped and pointed bubbles, which is five times larger than the average error on the pressure of $\Delta P = 3$ (see figure 8). The long fingers are associated with scatter in the pressure data, which is slightly larger than the average error on the pressure. This is attributed to the considerable variation in the length of their precursor finger.

4. Transition between states

4.1. *Symmetric to asymmetric bubbles*

For $(A/A_0)_{owc} < A/A_0 \leqslant 0.26$, symmetric bubbles were only found at low values of Ca, and the reflection symmetry of the bubble about the vertical mid-plane was broken as Ca was increased, as illustrated in figure 10. In the set of experiments shown in figure 10, a symmetric bubble was only observed for $Ca = 0.1$, the lowest value investigated. In order to quantify the asymmetry, the aerial image of the bubble tip was separated into two regions by an axial line originating at the most advanced point on the bubble. The bubble tip was delimited by a transverse line located 11.2 mm behind the apex of the bubble, which was positioned so that it included the entire tip for all the values of Ca investigated. As shown in figure 10, S_2 (S_1) is the area of the tip-region that grows (shrinks) with increasing asymmetry. The measure of the asymmetry, β, was defined as $0 \leqslant \beta = S_2/(S_1 + S_2) - 0.5 < 0.5$, where the subtracted value of 0.5 corresponds to the normalized value of S_2 for a symmetric bubble.

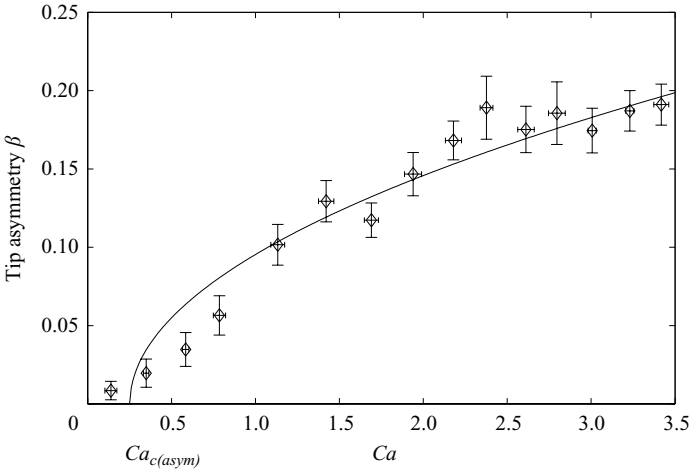

FIGURE 11. Variation of the tip asymmetry, β, with Ca, from experiments performed at $A/A_0 = 0.26$. The solid line is a fit of the form $\beta = M(Ca - Ca_{c(asym)})^{1/2}$, with $M = 0.11$ and $Ca_{c(asym)} = 0.25$, the critical value for the onset of asymmetric bubbles. The average error between the measured and the fitted values of β is 1.5×10^{-2}.

The variation of β with Ca in figure 11 shows the continuous growth of the asymmetry. The values shown are all positive, as the air bubbles in this series of experiments all propagated with a right-hand side bias, corresponding to the migration of the bubble tip into the upper part of the snapshot in figure 10(b). A least-square fit of the form $\beta^2 = M^2(Ca - Ca_{c(asym)})$, where $Ca_{c(asym)}$ is the critical capillary number beyond which asymmetric bubbles arise, gives $M = 0.11$ and $Ca_{c(asym)} = 0.25$, with an average error on β^2 of 4.0×10^{-3}. The approximate square-root dependence of the asymmetry on Ca suggests that the symmetric bubble loses stability to the asymmetric one through a supercritical pitchfork bifurcation (i.e. the simplest type of symmetry-breaking bifurcation). Although only the upper branch of the pitchfork was obtained at $A/A_0 = 0.26$, both right- and left-hand sides propagating bubbles were found for other levels of collapse (see figure 12), suggesting the existence of a lower branch of the pitchfork, which would be disconnected due to imperfections.

The bubble asymmetry is closely associated with the non-uniform shapes of the collapsed cross-sections, which are illustrated in figure 5 for decreasing values of A/A_0. The shear stresses in the lobes are smaller than those in the more collapsed central part of the cross-section, and thus the bubble tip deforms to promote propagation in either of the two lobes. This mechanism has been verified in rigid tubes with a partially occluded cross-section that is symmetric about the vertical mid-plane, and similar asymmetric bubbles are observed for increasing Ca (de Lózar *et al.* 2009).

4.2. *Asymmetric to double-tipped bubbles*

In figure 12, a series of top-view snapshots of the propagating bubble for $0.2 \leqslant Ca \leqslant 1.0$ illustrates the evolution of the asymmetric bubble and the transition to double-tipped bubbles at $A/A_0 = 0.13$. Five experiments were performed at each flow rate and the pictures in figure 12 were selected to show that the bubble could propagate down either of the side lobes. Note that the asymmetry of the tip is more pronounced than that for $A/A_0 = 0.26$ as shown in figure 10. As Ca increases, the asymmetric tip shortens, as highlighted with solid lines in figures 12(a) and 12(d), and

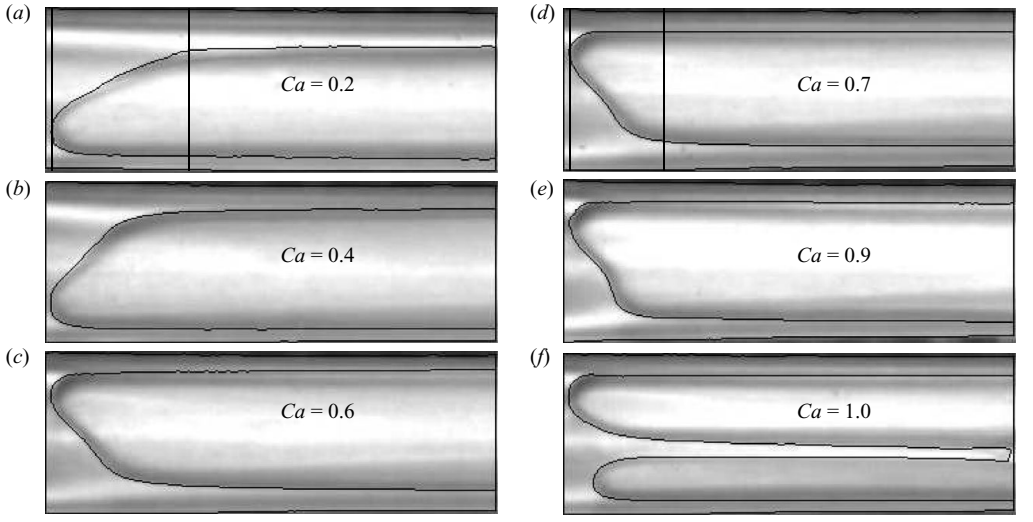

FIGURE 12. Series of top-view snapshots of reopening bubbles at $A/A_0 = 0.13$ for $0.2 \leqslant Ca \leqslant 1.0$. The tip of the asymmetric bubble (demarcated by vertical lines in (*a*) and (*d*)) shortens with increasing Ca, and a sudden transition to double-tipped bubbles is observed at $Ca = 1.0$.

its central part develops a shallow indentation at $Ca = 0.6$. Note that this indentation does not bear any relation to tip splitting in viscous fingering (Tabeling, Zocchi & Libchaber 1987), as it does not evolve during the propagation of the bubble. Moreover, it grows only slightly up to $Ca = 0.9$, beyond which the double-tipped bubble is formed, which comprises two fingers separated by a narrow liquid bridge that merge into the main bubble at a distance L_p behind the tips (Heap & Juel 2008). The dramatic change in bubble shape between figures 12(*e*) ($Ca = 0.9$) and 12(*f*) ($Ca = 1.0$) suggests a discontinuous transition between the asymmetric and double-tipped reopening states, which is documented in detail below. This interpretation is further supported by the existence of mixed states near the transition, as mentioned in § 3.1.2, where double-tipped bubbles suddenly switched to asymmetric bubbles during the course of an experiment at fixed values of A/A_0 and of the imposed flow rate Q.

The radical change in bubble shape at the transition between asymmetric and double-tipped bubbles was all the more unexpected, given that the transition could not be identified from the pressure data shown in figure 7. The side-view snapshots in figure 13 show an asymmetric bubble ($Ca = 0.9$) and a double-tipped bubble ($Ca = 1.0$) that were both obtained at $Q = 300\,\mathrm{cm^3\,min^{-1}}$. The length of the reopening region and the height of the reopened tube are similar in both cases to within experimental error, confirming the similarities of these two reopening processes. The free surface of the propagating bubble tip, however, increases dramatically with the onset of the double-tipped bubble. Thus, double-tipped bubbles may arise at larger values of Ca than required for asymmetric bubbles, because of the reduced influence of surface tension forces. However, stable double-tipped bubbles have also been found numerically by Heil (1999) at $Ca = 0$, but his three-dimensional model imposed a reflection symmetry about the vertical mid-plane.

The length of the fingers of the double-tipped bubble L_p defined schematically in figure 13(*b*) and measured in units of the inner diameter of the tube ($2R$) is plotted against Ca in figure 14. The experiments reported in figure 14(*a*) for $A/A_0 = 0.05$ focus on the lower range of Ca close to the transition to asymmetric bubbles, where

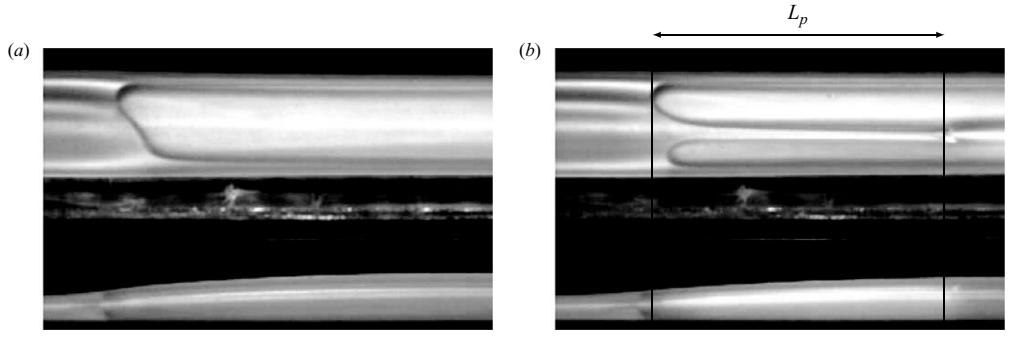

FIGURE 13. Top and side views from two experiments performed at $Q = 300\,\mathrm{cm}^3\,\mathrm{min}^{-1}$ with $A/A_0 = 0.13$: (*a*) asymmetric bubble ($Ca = 0.9$), (*b*) double-tipped bubble ($Ca = 1.0$). Note that the small differences in reopening heights and Ca are within the experimental variability.

L_p rises steeply to up to more than 30 tube diameters as Ca is reduced. Even longer precursor fingers extending up to the entire length of the tube were occasionally found, although L_p could not be measured in these cases for technical reasons. These findings suggest that L_p tends to infinity as Ca is reduced towards a critical threshold, $Ca_{c(dt)}$. An estimate of $Ca_{c(dt)}$ was obtained by fitting the data to the simplest function that asymptotes $Ca_{c(dt)}$, of the form $Ca - Ca_{c(dt)} = N(L_p/2R)^{-1}$. We find $N = 0.33$ and $Ca_{c(dt)} = 0.53$, but it yields a relatively large average error on Ca of 0.13. The diverging length of the liquid bridge joining the two precursor fingers is reminiscent of the diverging menisci that are shown to form in the corners of polygonal tubes in the absence of gravity by Concus & Finn (1974), when the contact angle of the liquid and the polygonal geometry are chosen so that a continuous equilibrium contact line does not exist. The comparison between values of L_p at $A/A_0 = 0.13$ and 0.05 in figure 14(*b*) suggests that the value of $Ca_{c(dt)}$ increases with A/A_0. It also points to a similar increase in the critical value of Ca beyond which pointed bubbles are found, so that the range over which double-tipped bubbles are observed does not vary significantly.

A comparison between the side views of tubes reopening with double-tipped bubbles at $Ca = 1.0$ and $Ca = 2.7$, respectively, is shown in figure 15 for $A/A_0 = 0.13$. As Ca increases, increasing heights of reopening coupled to a reopening region of approximately constant length, leads to the steepening of tube profile in the reopening region. The vertical line (i) indicates the location of the leading precursor finger tip, whereas the lines (ii) indicate the points of merging of the precursor fingers. The height of the reopened tube is compared with the height at which the precursor fingers of the double-tipped bubble merge in figure 16. At $Ca = 1.0$ the precursor fingers are considerably longer compared with $Ca = 2.7$, but the height of the tube at the point of merging is approximately the same. In fact, the height of reopening at the point of merging of the fingers (in units of inner tube diameter, $2R$) is approximately constant and equal to $h_{c(A/A_0=0.13)} = 0.59 \pm 0.03$ and $h_{c(A/A_0=0.05)} = 0.53 \pm 0.02$ for $A/A_0 = 0.13$ and 0.05, respectively. The error quoted corresponds to the standard deviation of the data. Double-tipped bubbles disappear when the tube reopens to a height less than or equal to the height at which the fingers would merge. The value h_c is expected to depend on the elastic properties of the tube as well as the level of collapse.

4.3. *Double-tipped to pointed bubbles*

As Ca increases, the length of the precursor fingers of the double-tipped bubbles decreases until it reaches a minimum value of approximately $L_{p(min)} \sim h_c$ at a critical

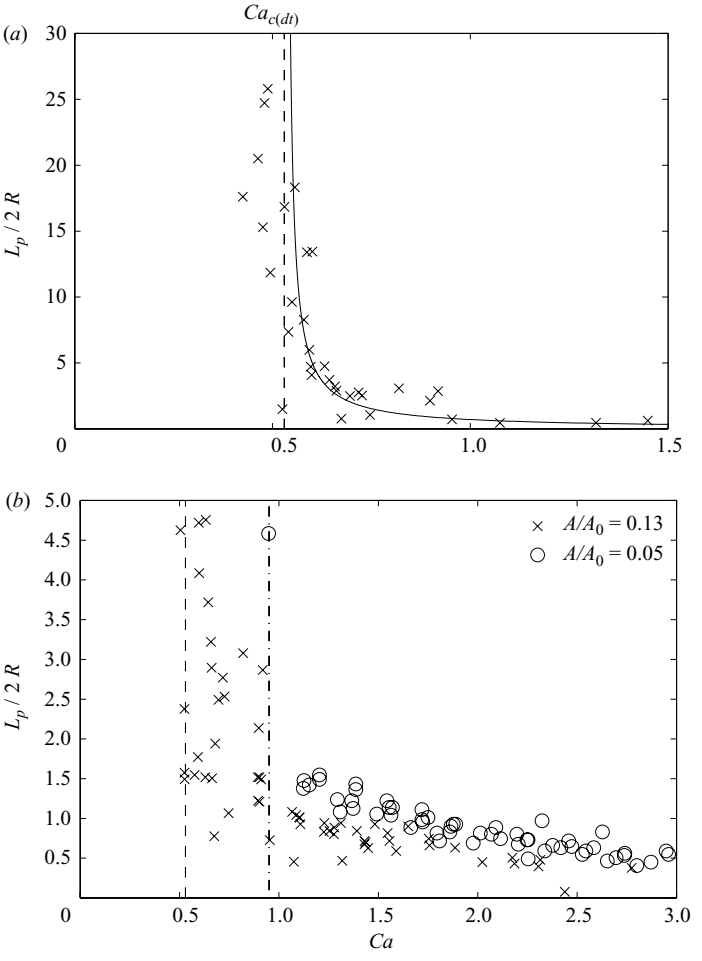

FIGURE 14. Variation of the length of the fingers in the double-tipped bubble with Ca: (*a*) $A/A_0 = 0.05$, for values of Ca close to the threshold below which asymmetric bubbles are observed. The solid line is a hyperbolic fit plotted to highlight the divergence of the data at a finite value of Ca. It is given by $Ca - Ca_{c(dt)} = N(L_p/2R)^{-1}$ with $N = 0.33$ and $Ca_{c(dt)} = 0.53$, the critical value for the onset of double-tipped bubble. It is associated with an average error on Ca of 0.13. (*b*) $A/A_0 = 0.13$ and 0.05, over the entire range of Ca where double-tipped bubbles are observed. The vertical line for $A/A_0 = 0.13$ marks the minimum value of Ca for which double-tipped bubbles were observed. The transition to pointed bubbles occurs when $L_p \lesssim 0.5$, i.e. less than one tube radius (see § 4.3).

value of the capillary number $Ca_{c(p)}$ (see figure 14). For $Ca > Ca_{c(p)}$, pointed bubbles are selected instead of the double-tipped bubble. An interpretation of this observation is that precursor fingers cannot be supported when the reopening region becomes excessively steep. The replacement of the double-tipped bubble by a pointed bubble is associated with a discontinuous reduction of the bubble pressure as shown in figure 7. This pressure reduction is coupled to an increase of the bubble speed, because experiments were performed at constant flow rate.

In figure 17, a comparison between double-tipped and pointed bubbles obtained for the same value of the flow rate $Q = 1300\,\mathrm{cm^3\,min^{-1}}$ at $A/A_0 = 0.13$ highlights important differences in the respective reopening processes. Whereas the central

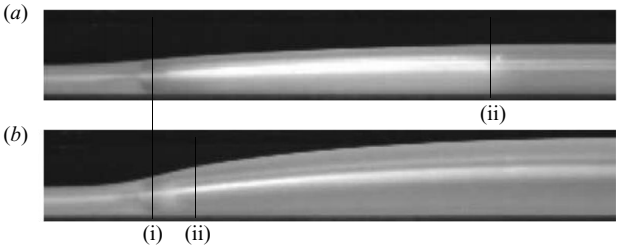

FIGURE 15. Side view of the transition region in tubes reopening with double-tipped bubbles for $A/A_0 = 0.13$: (*a*) $Ca = 1.0$, (*b*) $Ca = 2.7$. The vertical line (i) indicates the location of the leading finger tip, and the lines (ii) indicate the point of merging of the tips into the main reopening bubble.

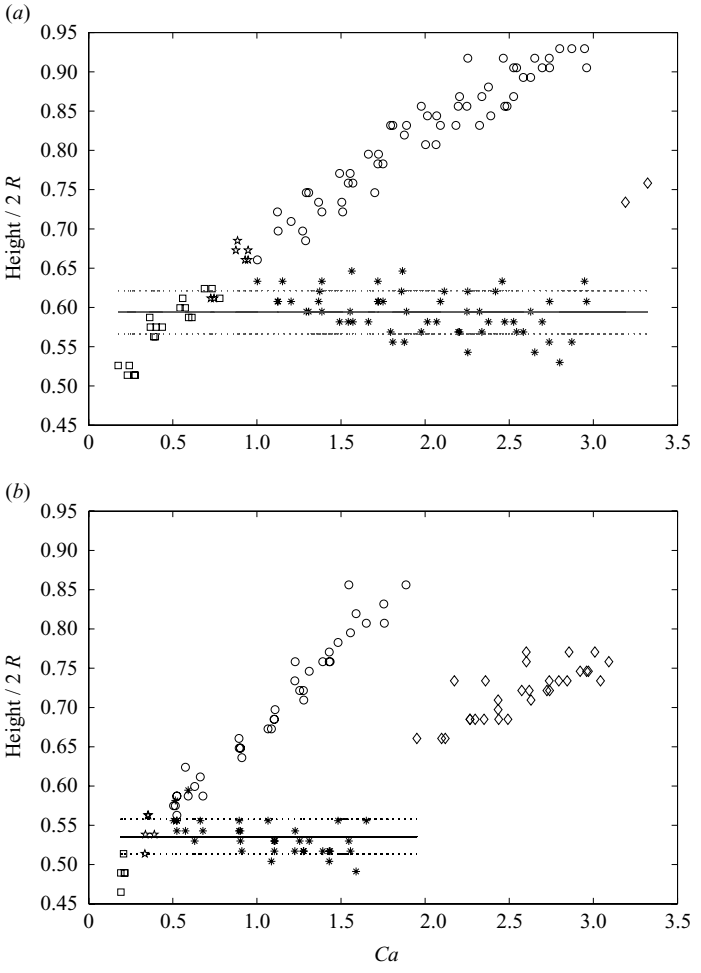

FIGURE 16. Variation of the height of the reopened tube (in units of inner tube diameter, $2R$) with Ca: (*a*) $A/A_0 = 0.13$, (*b*) $A/A_0 = 0.05$. The symbols represent symmetric (□), mixed double-tipped to asymmetric (pentagram), double-tipped (○) and pointed (◇) bubbles. The height of the tube at the axial location where the precursor fingers of the double-tipped bubble merge is shown with stars (*). This height is approximately constant with Ca and its mean value and standard deviations are shown with solid and dotted horizontal lines respectively. The double-tipped finger is unstable when the tube reopens to a height less or equal to the height at which the fingers would merge.

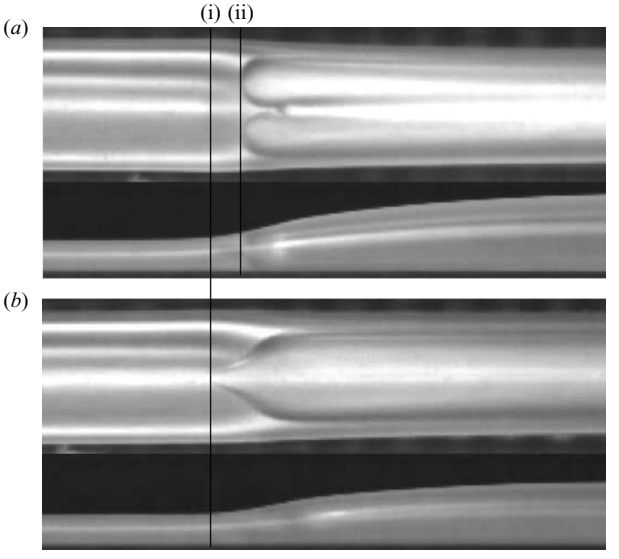

FIGURE 17. Comparison between double-tipped ($Ca = 3.0$) and pointed bubbles ($Ca = 3.3$) near transition for $A/A_0 = 0.13$. Both bubbles were obtained in experiments at $Q = 1300\,\mathrm{cm^3\,min^{-1}}$. The vertical line (i) in the snapshots indicates the point beyond which the tube remains collapsed. The cusp-shaped protrusion of the pointed finger extends to this point (i), while the tips of the double-tipped bubble are less advanced at location (ii), suggesting important differences in the flows ahead of the bubble tips. Note the larger height of reopening in (*a*) compared to (*b*), which is consistent with the larger double-tipped bubble pressures shown in figure 7.

protrusion on the pointed bubble extends into the collapsed region, the tips of the precursor fingers in the double-tipped bubble are set back as shown by the vertical line (ii). This is a further indication that they propagate by redistributing the fluid ahead of them, while the pointed finger overcomes large shear forces by infiltrating the most collapsed region. The pointed bubbles observed by Petitjeans & Maxworthy (1996) in miscible displacement flows with small bubble velocities are associated with the presence of recirculations ahead of the bubble that draw out fluid in the centre of the tube. We could not ascertain whether flows recirculations were responsible for focusing the interfacial flow into a pointed bubble, as we were unable to visualize the flow directly. However, whereas asymmetric and double-tipped bubbles can form in rigid tubes with non-uniform cross-sectional shapes (Heil 1999; de Lózar *et al.* 2009), the infiltration of the pointed bubble tip into the most collapsed region where shear forces are largest is unlikely in rigid tubes. Thus, we speculate that the formation of pointed bubbles is inherently linked to the reopening process.

5. Conclusion

We have presented the results of an investigation into the selection of reopening bubbles, which propagate into a strongly collapsed benchtop model of airway reopening. A recent review of the modelling of airway collapse (Heil *et al.* 2008) suggests that extensive collapse featuring opposite wall contact may be widespread in the lungs, particularly in the peripheral airways. The non-dimensional surface tension of these vessels is quoted to be $\sigma = 50$ (Hazel & Heil 2003), which is more than two orders of magnitude larger than in the case of our relatively stiff experimental tube.

Yet, the robustness of the peeling solution simulated for moderate initial collapse over this wide range of σ suggests that our findings may be relevant to pulmonary reopening processes.

We find that the level of collapse at which opposite wall contact first occurs within the tube cross-section is a critical threshold beyond which the reopening mechanics change qualitatively. For dimensionless cross-sections $A/A_0 \leqslant (A/A_0)_{owc} = 0.18$, the canonical parabolic-tipped peeling bubble is replaced by 'asymmetric' and 'double-tipped', whose pressure is set in the lobes of the collapsed tube, while the pressure of 'pointed' bubbles is proportional to the width of the central thin-film region. For near-complete collapse, $A/A_0 \leqslant 0.04$, two further types of bubbles are observed: 'long asymmetric' and 'long double-tipped', which are both defined by the long precursor finger that propagate within one of the lobes without affecting the opposite wall contact of the cross-section.

The supercritical breaking of the bubble symmetry about the vertical mid-plane is observed for collapsed cross-sectional areas as large as $A/A_0 = 0.26$, at which the opposite walls of the collapsed cross-section are not in contact. The resulting asymmetric bubbles may impact the dynamics at airway bifurcations, leading to the preferential reopening of one daughter vessel over the others. Double-tipped bubbles are formed instead of asymmetric ones when the tube reopens to a height at least equal to the height at which precursor fingers merge into the main bubble. In turn, the double-tipped bubble disappears beyond a critical steepness of the reopening region. It is replaced by the pointed bubble, which is a faster bubble of significantly lower pressure. This pointed bubble may be relevant physiologically, as closed airways must be reopened quickly without damaging the fragile tissues that line them (Ghadiali & Gaver 2008).

The authors wish to thank G. Dawson and M. North for their help with the measurements of Figure 14. They are grateful to Dr M. Heil and Dr A. L. Hazel for many useful discussions and valuable comments during the preparation of this manuscript. They also thank the referees for their detailed comments that have improved the manuscript. This work was funded by the EPSRC (A. Heap) and an EPSRC 'Advanced Research Fellowship' (A. Juel).

REFERENCES

Bland, R. D. 1991 Fetal lung liquid and its removal near birth. In *The Lung: Scientific Foundations* (ed. R. G. Crystal, J. B. West, P. J. Barnes & E. R. Weibel). Lippincott, Williams and Wilkins.

Bretherton, F. P. 1961 The motion of long bubbles in tubes. *J. Fluid Mech.* **10**, 166–188.

Cohen, I. & Nagel, S. R. 2002 Scaling at the selective withdrawal transition through a tube suspended above the fluid surface. *Phys. Rev. Lett.* **88**, 074501.

Concus, P. & Finn, R. 1974 On capillary free surfaces in the absence of gravity. *Acta Mathematica* **132**, 177–198.

Courrech du Pont, S. & Eggers, J. 2006 Sink flow deforms the interface between a viscous liquid and air into a tip singularity. *Phys. Rev. Lett.* **96**, 034501.

Fearn, R. 1988 Perturbed motions of a bubble rising in a vertical tube. *Phys. Fluids* **31**, 238–241.

Flaherty, J. E., Keller, J. B. & Rubinow, S. I. 1972 Post-buckling behaviour of elastic tubes and rings with opposite sides in contact. *SIAM J. Appl. Math.* **23**, 446–455.

Gaver III, D. P., Halpern, D., Jensen, O. E. & Grotberg, J. B. 1996 The steady motion of a semi-infinite bubble through a flexible-walled channel. *J. Fluid Mech.* **319**, 25–65.

Gaver III, D. P., Samsel, R. W. & Solway, J. 1990 Effects of surface tension and viscosity on airway reopening. *J. Appl. Physiol.* **69**, 74–85.

Ghadiali, S. & Gaver, D. P. 2008 Biomechanics of liquid–epithelium interactions in pulmonary airways. *Respir. Physiol. Neurobiol.* **163**, 232–243.

Grotberg, J. B. 2001 Respiratory fluid mechanics and transport processes. *Ann. Rev. Biomech. Engng* **3**, 421–457.

Grotberg, J. B. & Jensen, O. E. 2004 Biofluid mechanics in flexible tubes. *Ann. Rev. Fluid Mech.* **36**, 121–147.

Hazel, A. L. & Heil, M. 2002 The steady propagation of a semi-infinite bubble into a tube of elliptical or rectangular cross-section. *J. Fluid Mech.* **470**, 91–114.

Hazel, A. L. & Heil, M. 2003 Three-dimensional airway reopening: the steady propagation of a semi-infinite bubble into a buckled elastic tube. *J. Fluid Mech.* **478**, 47–70.

Hazel, A. L. & Heil, M. 2006 Finite-Reynolds-number effects in steady, three-dimensional airway reopening. *ASME J. Biomech. Engng* **128**, 573–578.

Hazel, A. L. & Heil, M. In press The influence of gravity on the steady propagation of a semi-infinite bubble into a flexible channel. *Phys. Fluids* **20**, 092109.

Heap, A. & Juel, A. 2008 Anomalous bubble propagation in elastic tubes. *Phys. Fluids* **20**, 081702.

Heil, M. 1999 Minimal liquid bridges in non-axisymmetrically buckled elastic tubes. *J. Fluid Mech.* **380**, 309–337.

Heil, M., Hazel, A. L. & Smith, J. A. 2008 The mechanics of airway closure. *Respir. Physiol. Neurobiol.* **163**, 214–221.

Hong, D. 1988 Wire perturbations in the Saffman–Taylor problem. *Phys. Rev.* A **37**, 2724–2727.

Jensen, O. E., Horsburgh, M. K., Halpern, D. & Gaver III, D. P. 2002 The steady propagation of a bubble in a flexible-walled channel: asymptotic and computational models. *Phys. Fluids* **14**, 443–457.

Juel, A. & Heap, A. 2007 The reopening of a collapsed fluid-filled elastic tube. *J. Fluid Mech.* **572**, 287–310.

Kamm, R. D. 1999 Airway wall mechanics. *Ann. Rev. Biomech. Engng* **1**, 47–72.

Kuang, J., Petitjeans, P. & Maxworthy, T. 2004 Velocity fields and streamline patterns of miscible displacements in cylindrical tubes. *Exp. Fluids* **37**, 301–308.

Lorenceau, E., Restagno, F. & Quéré, D. 2003 Fracture of a viscous liquid. *Phys. Rev. Lett.* **90**, 184501.

de Lózar, A., Heap, A., Box, F., Hazel, A. L. & Juel, A. 2009 Partially-occluded tubes can force switch-like transitions in the behavior of propagating bubbles. *Phys. Rev. Lett.* Submitted.

Perun, M. L. & Gaver III, D. P. 1995 An experimental model investigation of the opening of a collapsed untethered pulmonary airway. *ASME J. Biomech. Engng* **117**, 245–253.

Petitjeans, P. & Maxworthy, T. 1996 Miscible displacements in capillary tubes. Part I. Experiments. *J. Fluid Mech.* **326**, 37–56.

Tabeling, P., Zocchi, G. & Libchaber, A. 1987 An experimental study of the Saffman–Taylor instability. *J. Fluid Mech.* **177**, 67–82.

Taylor, G. I. 1961 Deposition of a viscous fluid on the wall of a tube. *J. Fluid Mech.* **10**, 161–165.